Journal of Biomedical Optics 9(5), 1018–1027 (September/October 2004)

In vivo assessment of thermal damage in the liver using optical spectroscopy

Clay R. Buttemere
Vanderbilt University
Department of Biomedical Engineering
Nashville, Tennessee 37235

Ravi S. Chari
Christopher D. Anderson
Vanderbilt University Medical Center
Department of Surgery
Nashville, Tennessee 37235

M. Kay Washington
Vanderbilt University Medical Center
Department of Medical Pathology
Nashville, Tennessee 37235

Anita Mahadevan-Jansen
Wei-Chiang Lin
Vanderbilt University
Department of Biomedical Engineering
Nashville, Tennessee 37235
E-mail: wei-chiang.lin@vanderbilt.edu

Abstract. Resection is not a viable treatment option for the majority of liver cancer patients. Alternatives to resection include thermotherapies such as radio-frequency ablation; however, these therapies lack adequate intraoperative feedback regarding the degree and margins of tissue thermal damage. In this proof of principle study, we test the ability of fluorescence and diffuse reflectance spectroscopy to assess local thermal damage *in vivo*. Spectra were acquired *in vivo* from healthy canine liver tissue undergoing radio-frequency ablation using a portable fiber-optic-based spectroscopic system. The major observed spectral alterations on thermal coagulation were a red shift in the fluorescence emission peak at 480 nm, a decrease in the overall fluorescence intensity, and an increase in the diffuse reflectance from 450 to 750 nm. Spectral changes were quantified and correlated to tissue histology. We found a good correlation between the proposed spectral correlates of thermal damage and histology. The results of this study suggest that fluorescence and diffuse reflectance spectroscopy show strong potential as tools to monitor liver tissue thermal damage intraoperatively.
[DOI: 10.1117/1.1779627]

Keywords: diffuse reflectance; fluorescence spectroscopy; radio-frequency ablation; thermotherapies.

Paper 03049 received Apr. 22, 2003; revised manuscript received Aug. 5, 2003; accepted for publication Jan. 30, 2004.

1 Introduction

Currently, one of the limitations of cancer treatment modalities that use heat to achieve tumor necrosis is the lack of intraoperative feedback regarding the degree and margins of tissue thermal damage. These therapies (e.g., radio-frequency ablation) are being used increasingly in the treatment of liver cancer patients, since 80 to 95% of them are not candidates for standard surgical resection.[1,2] Local tumor recurrence rates are one measure of the efficacy of these therapies. For example, local tumor recurrence rates of 4 to 19% have been reported for radio-frequency ablation (RFA) of unresectable liver tumors.[1–7] The development of a feedback system that provides clinicians with an objective therapeutic endpoint could potentially improve local tumor recurrence rates and, consequently, long-term patient survival rates.

Several feedback systems for liver tumor thermotherapies have been proposed and investigated in the past. Thermocouple systems[8,9] and intraoperative MRI[10–12] use local temperature measurements as a metric of thermal damage. There are already some RFA systems using thermocouples embedded in the electrode arrays to monitor local tissue temperatures and modulate ablation power to achieve large ablation zones. However, according to the Arrhenius model,[13] thermal damage is a rate process that depends not only on the local temperature-time history of the tissue, but also on tissue-specific empirical constants. Therefore, local temperature measurements are of limited predictive value if they are not considered in a broader context, such as the Arrhenius model. Ultrasound[14–16] and light transmission[17,18] have also been proposed as ways to assess tissue thermal damage intraoperatively. However, both of these approaches are hampered by problems such as poor spatial resolution and sensitivity.

Previously, we reported on the fluorescence and diffuse reflectance spectral alterations that occur in liver tissue during thermal coagulation *in vitro*.[19] In that study, the observed changes in spectral features were correlated to theoretical thermal damage predictions made using the Arrhenius thermal damage model.[13] The time courses of the spectral features generally agreed with the model-predicted thermal damage time courses. The goal of the current study is to validate the spectral changes associated with thermal coagulation *in vitro* in an *in vivo* setting. To that end, fluorescence and diffuse reflectance spectra were acquired from liver tissue being coagulated using RFA *in vivo*, and spectral changes were correlated to histological evaluations of the optical interrogation sites. Results obtained from this study indicate that fluorescence and diffuse reflectance spectroscopy can assess the extent of tissue thermal damage *in vivo* and therefore have the potential to monitor liver thermotherapies such as RFA.

2 Materials and Methods

2.1 *Spectroscopic System*

A portable fiber-optic-based spectroscopic system (depicted in Fig. 1) was used to acquire fluorescence and diffuse reflec-

Address all correspondence to Wei-Chiang Lin, Dept. of Biomedical Engineering, Vanderbilt University, 5801 Stevenson Ctr., Nashville, TN 37235. Tel: 615-343-4190; Fax: 615-343-7919; E-mail: wei-chiang.lin@vanderbilt.edu

1083-3668/2004/$15.00 © 2004 SPIE

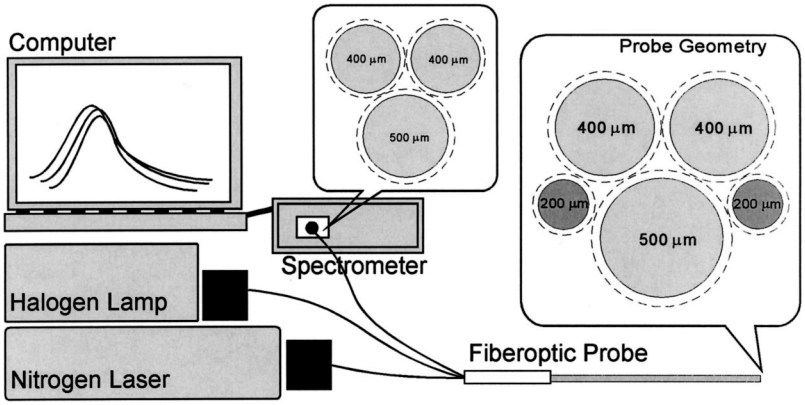

Fig. 1 The spectroscopic system and the geometry of the fiber optic probe. The shaded areas represent the core of the fibers and the dashed lines delineate the thickness of the cladding and protective buffer of the fibers. The 200-μm core fibers in the probe carry the excitation light, while the other fibers are used for collection.

tance spectra from liver tissue undergoing RFA. The fluorescence excitation light source used was a nitrogen laser emitting at 337 nm and operated at a repetition rate of 20 Hz (High Pressure Nitrogen Dye Laser, Oriel Corporation, Stratford, Connecticut). The average pulse energy of the laser was approximately 50 μJ (standard deviation = 15%) at the tissue surface. The selection of this excitation wavelength was based on previous excitation-emission matrix studies that indicated that the fluorescence emission of native and coagulated liver tissue differed significantly at 337-nm excitation.[19] The diffuse reflectance excitation light source was a 150-W halogen lamp (Fiber Lite, Model 180, Edmund Industrial Optics, Barrington, New Jersey).

A multifiber probe built in the Biomedical Optics Lab at Vanderbilt University was used for light delivery and collection. The probe consists of two 200-μm core excitation fibers, and two 400-μm and one 500-μm core collection fibers (UV Enhanced Silica Optical Fibers, Polymicro Technologies, Phoenix, Arizona) that are encased in a pointed 17-gauge stainless steel cannula with a 1.47-mm outer diameter. The collection fibers are coupled directly to a spectrometer (S2000-FL Spectrometer, Ocean Optics, Dunedin, Florida) with a spectral range of 350 to 1000 nm sampled nonlinearly over 2048 pixels. The spectrometer utilized in this *in vivo* study was equipped with a 200-μm slit at its entrance port, which yielded a spectral resolution of $\sim$10 nm. A long-pass filter with a cutoff at 385 nm is installed at the entrance to the spectrometer to prevent reflected fluorescence excitation light from reaching the detector. The spectrometer interfaces with an A/D converter that connects to a laptop computer via a USB interface (ADC1000-USB A/D Converter, Ocean Optics, Dunedin, Florida). Proprietary software (OOIBase32, Ocean Optics, Dunedin, Florida) was used to control the spectrometer and acquire the data. An integration time of 1 s was used throughout the study, which provided sufficient signal-to-noise ratios. An interval of 5 s between spectral acquisitions was used, which was found to provide adequate temporal sampling of the ablation process that usually lasted 2 to 5 min.

2.2 *Experimental Procedure*

Acute RFA studies approved by the Vanderbilt University Institutional Animal Care and Use Committee (IACUC) were conducted on adult dogs. Induction and maintenance of anesthesia were accomplished using sodium pentothal (induction, intravenous injection, 15 mg/kg) and isofluorane (maintenance, inhalation, 1.5 to 2.5% in O_2). Following a midline laparotomy, control measurements were made in which fluorescence and diffuse reflectance spectra were acquired every 5 s over a 5-min period with the fiber-optic probe inserted into a deep region of parenchymal liver tissue, but without rf energy being delivered. Then, the RFA probe (StarBurst Electrosurgical Device, RITA Medical Systems, Mountain View, California) was inserted into a different deep region of liver tissue and deployed such that an ablation zone of 2 to 3 cm diam could be achieved. Using palpation of the liver surface and visual cues, such as the angle of insertion of the RFA probe, the fiber-optic probe was inserted into the expected zone of ablation, as shown in Fig. 2. The RFA generator (Model 1500X, RITA Medical Systems, Mountain View, California) was operated in a constant power mode (80 W) with the temperature-feedback control feature of the system disabled.

Ablation was performed at up to six sites per animal. At any given ablation site, either fluorescence or diffuse reflectance spectra were acquired continuously at a fixed point inside the estimated zone of ablation over the entire ablation

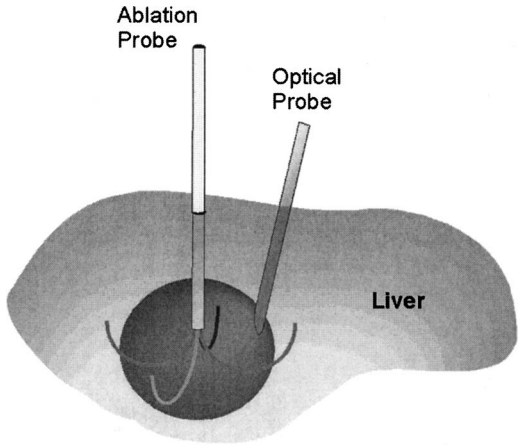

Fig. 2 The placement of the optical probe within the electrode array of the RFA probe.

Table 1 Tissue thermal damage scoring system.

Microhistology		Gross histology		Composite score
Feature	Score	Position of probe tip	Score	
Hemorrhage	1 or 2			
Blood coagulation	3	Inside ZOA (high-grade)	2	
Sinusoidal dilatation	1	Edge of ZOA (intermediate-grade)	1	Microhistology score/3 + Gross histology score
Vacuole formation	1	Outside ZOA (undamaged/low-grade)	0	
Tissue fragmentation	1			

time course. Spectral data acquisition was also performed during the cooling phase to account for any reversible optical property changes induced by tissue heating.[20]

Temperatures were monitored using readings from the thermocouples embedded in the electrode tips, but were not used to control or guide therapy. Typical maximum temperatures achieved during ablation ranged from 60 to 110 °C. At least one set of fluorescence and diffuse reflectance data for each dog was acquired during a ''partial ablation,'' in which the delivery of rf energy was terminated before the spectral features of interest (e.g., peak intensity) reached a plateau.

After each ablation, the location of the optical probe tip was registered using a small amount of India ink delivered via a hypodermic needle that was inserted along the optical probe track. Following the last ablation site, the dog was euthanized using sodium pentobarbital (125 mg/kg, intravenous injection). The surgical time for each dog study was 1 to 2 h. The data presented in this work are from six dog studies that yielded a total of 15 sets of fluorescence data and 14 sets of diffuse reflectance data.

2.3 *Spectral Processing and Analysis*

The fluorescence and diffuse reflectance spectra were postprocessed to reduce spectral noise using a third-order Savitzky-Golay filter.[21] The window size of the filter was selected so as not to smooth over important spectral features such as the absorption peaks of oxyhemoglobin at 414, 542, and 576 nm.[22] Additionally, adjacent data points in the spectra were averaged to create 2-nm spacing along the wavelength axis and thereby made the size of the data array more manageable. The final wavelength ranges with adequate signal-to-noise ratios were found to be 400 to 650 nm and 450 to 750 nm for the fluorescence and diffuse reflectance spectra, respectively.

To account for the wavelength-dependent sensitivity of the spectroscopic system, all measured spectra were corrected using a set of calibration factors $C_S(\lambda)$ derived from a standard calibration procedure.[23] Diffuse reflectance spectra were further calibrated to account for the wavelength-dependent emissivity of the halogen lamp.[23] All calibrated spectra were then analyzed to identify the dominant changes that occurred during ablation. Next, prominent spectral changes were analyzed as a function of ablation time to determine appropriate metrics of those changes.

2.4 *Histological Processing and Analysis*

After each animal was euthanized, the tissue around each ablation zone was excised and sliced along a plane that exposed the optical probe track. A gross histology picture of the zone of ablation (ZOA) was taken and the location of the optical probe tip was registered using a small needle inserted perpendicular to the optical probe track. The tissue sample was then trimmed and fixed in a 10% formalin solution for at least 48 h before being sent to pathology for routine sectioning, hematoxylin and eosin staining, and evaluation.

For each ZOA, a representative tissue section (i.e., sample) was selected and a 4-mm-diameter circle was drawn on the microscope slide around the needle hole marking the optical interrogation site. This diameter was selected due to the inaccuracies inherent in the optical interrogation site registration technique (see Discussion in Sec. 4). Within this circle, an experienced pathologist searched for hallmarks of tissue thermal damage visible under a light microscope, including hemorrhage, blood coagulation, sinusoidal dilatation, extracellular vacuole formation, and tissue fragmentation.[13]

An arbitrary scoring system was established based on the gross and micro-histological features of the ablated liver samples (see Table 1); therefore, their degrees of thermal damage could be quantified. In this system, each sample received a ''microhistology score'' on a scale from 0 to 6 points, based on the microscopic markers of thermal damage. According to our definition, blood coagulation presupposes hemorrhage; therefore, samples could only receive points for one feature or the other, but not both. In samples where both hemorrhage and blood coagulation were present, the dominant (i.e., most pervasive) feature was scored. In addition, each sample was also given a ''gross histology score'' based on the location of the fiber-optic probe tip relative to the ZOA. Finally, the microhistology score was scaled to a maximum value of 2 and was added to the gross histology score to yield a composite thermal damage score on a scale of 0 to 4 points.

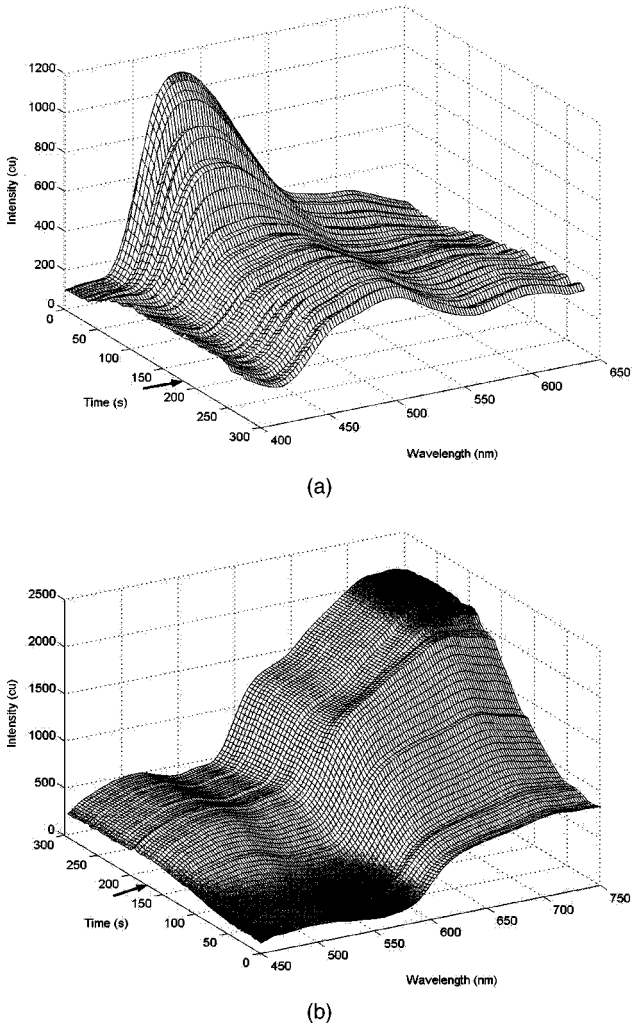

Fig. 3 The complete spectral time course for representative (a) fluorescence and (b) diffuse reflectance ablation sites. The arrows in (a) and (b) denote the cessation of rf current to the tissue. (cu = calibrated units.)

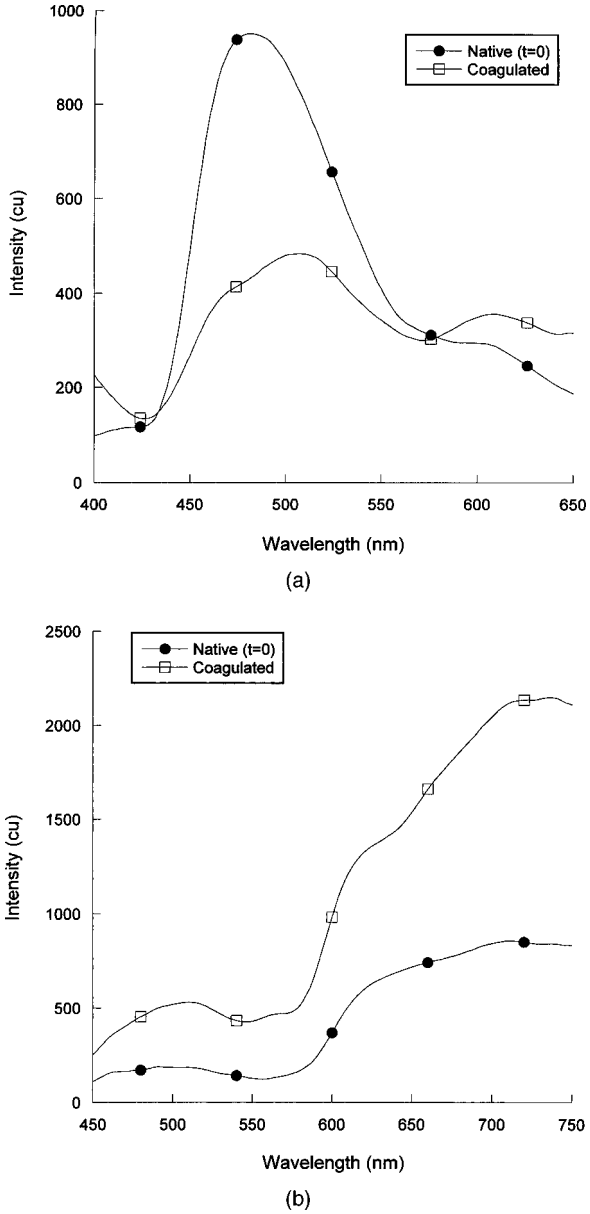

Fig. 4 The initial and final (a) fluorescence and (b) diffuse reflectance spectra for the same ablation sites as in Fig. 3. (cu = calibrated units.)

The composite scores were used to determine the degree of correlation between the observed spectral changes and tissue thermal damage.

Based on their gross histology score alone, the samples were divided into three grades of thermal damage. Samples with a score of 0 were classified as undamaged/low grade, samples with a score of 1 were classified as intermediate grade, and samples with a score of 2 were classified as high grade. This allowed for a statistical analysis of the spectral data within and among various grades of thermal damage.

3 Results

Fluorescence and diffuse reflectance spectra were measured *in vivo* from healthy canine liver tissue undergoing RFA. Time courses of fluorescence and diffuse reflectance spectra from two cases of severe (high-grade) thermal damage, as confirmed by histology, are shown in Figs. 3(a) and 3(b), respectively. The corresponding initial (i.e., native) and final (i.e., at the end of the data recording period) spectra from each set of data are plotted in Figs. 4(a) and 4(b). The advance of thermal damage gradually induced several alterations in both fluorescence and diffuse reflectance spectra from liver tissue. At these particular optical interrogation sites, the peak fluorescence intensity at 480 nm decreased by 45% and the peak location shifted to 508 nm, whereas the diffuse reflectance increased between 110 and 165% between 600 and 750 nm. Several other line shape changes were noted as well. A depression between 600 and 700 nm appeared in the diffuse reflectance signal at around the same time that the peak intensity was achieved. Finally, it was noted that the shoulder at 610 nm in the fluorescence spectra became more pronounced as the ablation progressed; however, the intensity at this wavelength remained relatively stable (standard deviation = 12% of mean intensity).

Three spectral correlates of thermal damage were defined based on the observed major spectral changes. For the fluo-

rescence data, two correlates were defined. To track the intensity decrease in the fluorescence emission peak, the ratio of the intensity at 610 nm to the intensity at 480 nm (F_{610}/F_{480}) was used. To track the fluorescence peak shift, the ratio of the intensity at 510 nm to the intensity at 480 nm (F_{510}/F_{480}) was used. For the diffuse reflectance data, the intensity at 720 nm (Rd_{720}) was selected to represent the increase in absolute intensity observed across the entire spectral range (450 to 750 nm). The selection of Rd_{720} was made based on the fact that the optical absorption of blood between 600 and 750 nm is 1 to 2 orders of magnitude less than the absorption between 450 and 600 nm. Therefore, the selection of an interrogation wavelength in a region of relatively weaker blood absorption allowed for detection of changes that were presumably related to the damage of hepatic tissue rather than damage to blood or changes in perfusion or oxygenation.

F_{510}/F_{480}, F_{610}/F_{480}, and Rd_{720} were analyzed as a function of ablation time. Representative time courses of the spectral correlates of thermal damage are shown in Figs. 5(a) and 5(b). All data points in a given time course were normalized to the initial (i.e., native) point for that dataset, which facilitated quantitative comparison among samples. In cases of severe thermal damage [e.g., data plotted in Figs. 5(a) and 5(b)], the time courses of all three spectral correlates of thermal damage exhibited two distinct phases: an initial ramp-up phase and a rapid increase phase. For cases of ''full ablation,'' the spectral correlates often plateaued prior to termination of rf ablation. This plateau phenomenon, however, was not observed in the cases of ''partial ablation.'' The dynamic range of the three normalized spectral correlates identified (maximum value–minimum value) varied. As seen in Fig. 5(a), normalized F_{610}/F_{480} has a dynamic range five times that of normalized F_{510}/F_{480}, even though both reach a stable plateau at around the same time. However, because the distance between the optical probe and the electrodes in the rf array was not fixed, the time to reach a stable plateau varied significantly from ablation site to ablation site. Due to this and other sources of variability, such as differences in tissue composition and local blood perfusion, histology was used as the standard against which the spectral correlates of thermal damage were evaluated.

To determine the degree of correlation between the spectral and histological data, scatter plots were created in which the final values of normalized F_{510}/F_{480}, F_{610}/F_{480}, and Rd_{720} and the composite thermal damage scores of the samples were compared (see Fig. 6). In general, the scatter plots indicate that the changes in spectral correlates, especially F_{510}/F_{480} and F_{610}/F_{480}, increase as the degree of thermal damage elevates. This is consistent with the trend derived from the dynamics of fluorescence and diffuse reflectance spectra shown in Fig. 3. In these scatter plots, two fluorescence samples and three diffuse reflectance samples (outliers, within dashed squares) are found vastly deviated from this trend. Based on the *in vitro* observations reported previously,[19] the dynamics of fluorescence and diffuse reflectance spectra illustrated in Fig. 3, and the inherent shortcomings of our optical interrogation site registration procedure, we suspect that the spectral and histological data for these samples may not be recorded from the same point in the ablation zone (i.e., the location of the optical probe tip was incorrectly identified).

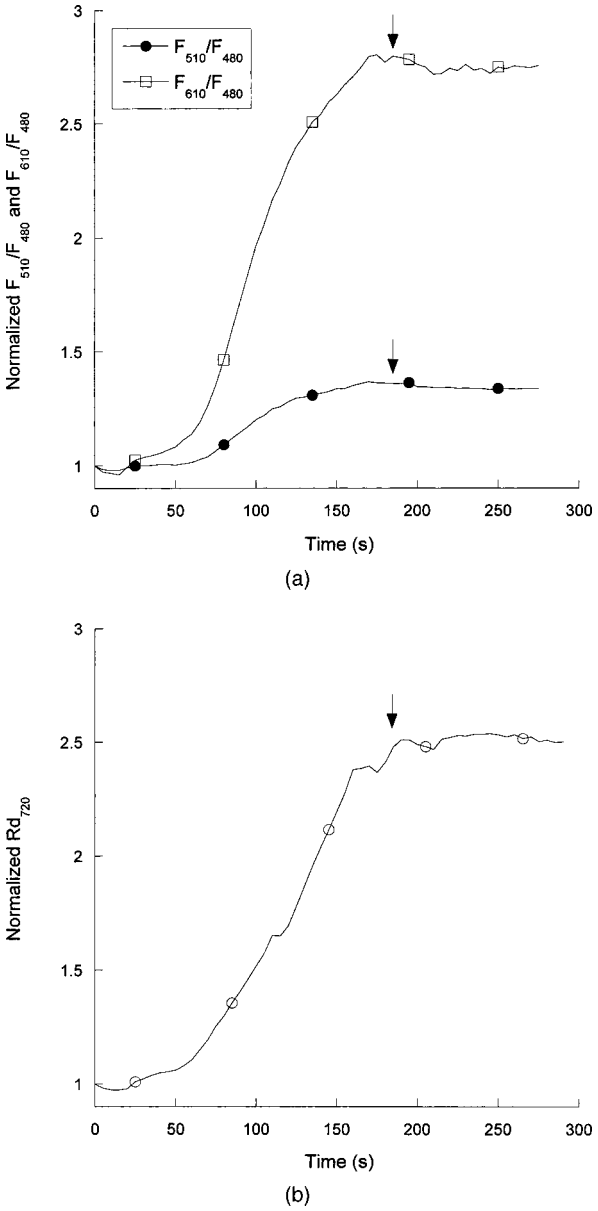

Fig. 5 The F_{510}/F_{480}, F_{610}/F_{480}, and Rd_{720} time courses for the same ablation sites as in Fig. 3. The arrows in (a) and (b) denote the cessation of rf current to the tissue. All data points in (a) and (b) are normalized to the initial data point.

The average final values of normalized F_{510}/F_{480}, F_{610}/F_{480}, and Rd_{720} and their corresponding standard deviations (SD) were computed for each grade of thermal damage as defined in Sec. 2. Note that the values of normalized F_{510}/F_{480} and F_{610}/F_{480} were computed from the same set of ablation sites, whereas the values of normalized Rd_{720} were computed from a completely different set of ablation sites. The results are shown in Table 2. The Student's t-test (one-tailed, two-sample, unequal variance) was used to determine if the mean F_{510}/F_{480}, F_{610}/F_{480}, and Rd_{720} in the high-grade group were significantly greater than those in the intermediate-grade and the undamaged/low-grade group, and if the intermediate-group means were significantly greater than the undamaged/low-grade means. For F_{510}/F_{480} and

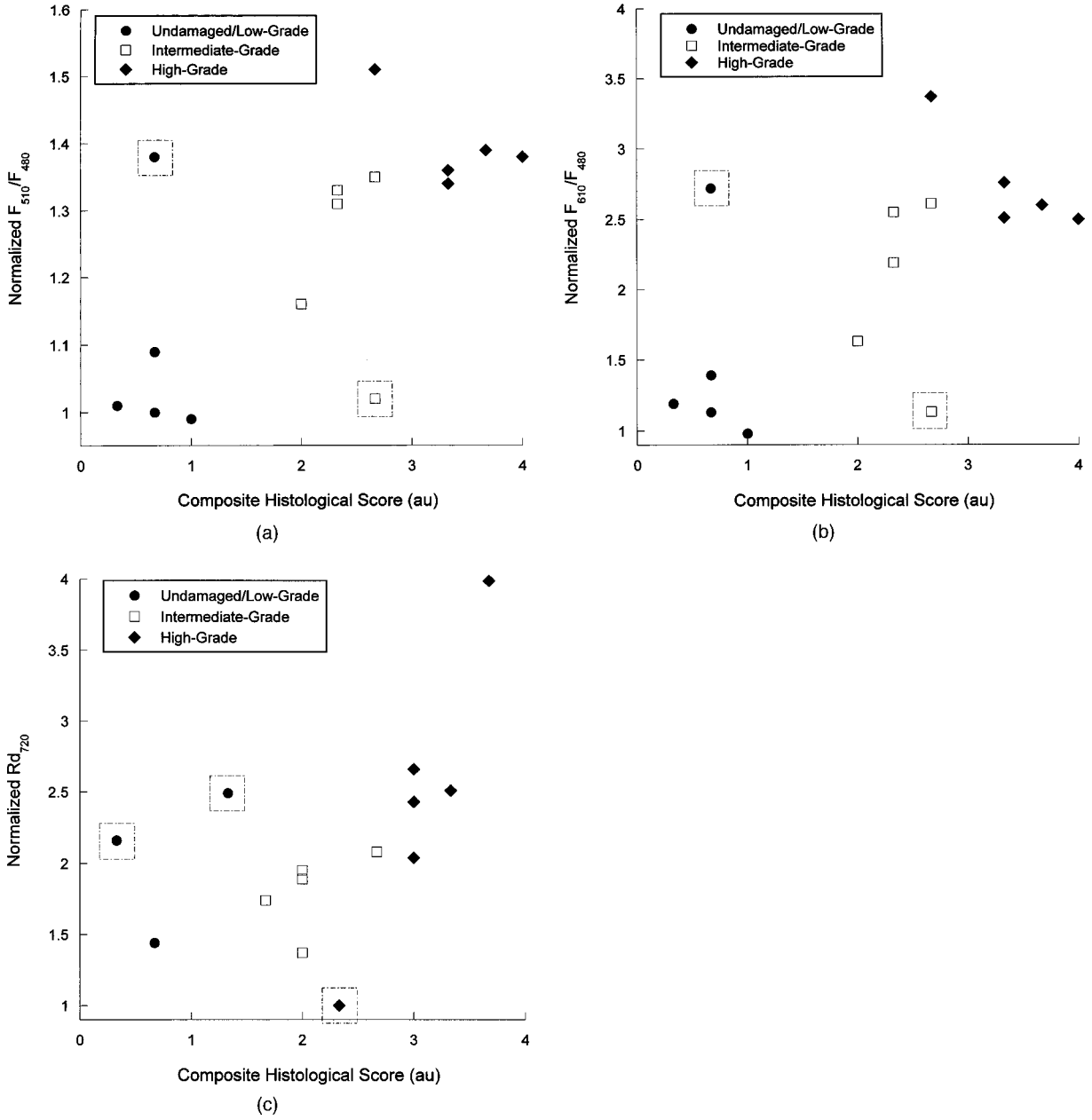

Fig. 6 The spectral feature versus histology plots for (a) F_{510}/F_{480}, (b) $F_{610/480}$, and (c) Rd_{720}. The outliers, situated in dashed squares, were included in the data analysis.

F_{610}/F_{480}, the significance levels for the high-grade group versus undamaged/low-grade group and intermediate-grade group were $p<0.05$. For Rd_{720}, only the comparison between the high- and intermediate-grade groups yielded a significance level of $p<0.1$.

Lastly, the line shape of native and coagulated liver tissue spectra obtained *in vivo* was compared to those obtained *in vitro*.[19] Figures 7 and 8 show this comparison for representative fluorescence and diffuse reflectance spectra, respectively. To help understand the differences between the native *in vitro* and *in vivo* spectra, the absorption spectra of oxy- and deoxy-hemoglobin[22] were plotted along with the liver tissue spectra. The native fluorescence spectra were found to have similar peak locations (490 nm *in vitro*, 480 nm *in vivo*); however, the full width at half maximum (FWHM) of the *in vivo* fluorescence peak was 90 nm as compared to a FWHM of 145 nm for the *in vitro* peak [Fig. 7(a)]. The major difference between the native diffuse reflectance spectra was a more pronounced valley between 500 and 600 nm observed *in vivo* [Fig. 7(b)]. A noticeable difference in line shape was found between the coagulated fluorescence spectra [Fig. 8(a)]; the *in vivo* one shows a secondary peak at 600-nm emission. As for the coagulated diffuse reflectance spectra, the *in vivo* one possessed a valley at ~650 nm that was not seen in the *in vitro* one [Fig. 8(b)].

Table 2 Spectral correlates of thermal damage.

Normalized final F_{510}/F_{480}						
Grade	Value	SD	*n*		*P*	
Undamaged/low	1.09	0.17	5	0.09		
Intermediate	1.24	0.14	5		0.03	0.006
High	1.39	0.07	5			
Normalized final F_{610}/F_{480}						
Grade	Value	SD	*n*		*P*	
Undamaged/low	1.48	0.71	5	0.1		
Intermediate	2.02	0.63	5		0.3	0.006
High	2.75	0.36	5			
Normalized final Rd_{720}						
Grade	Value	SD	*n*			
Undamaged/low	2.03	0.54	3	0.03		
Intermediate	1.92	0.37	6		0.09	0.2
High	2.44	0.94	5			

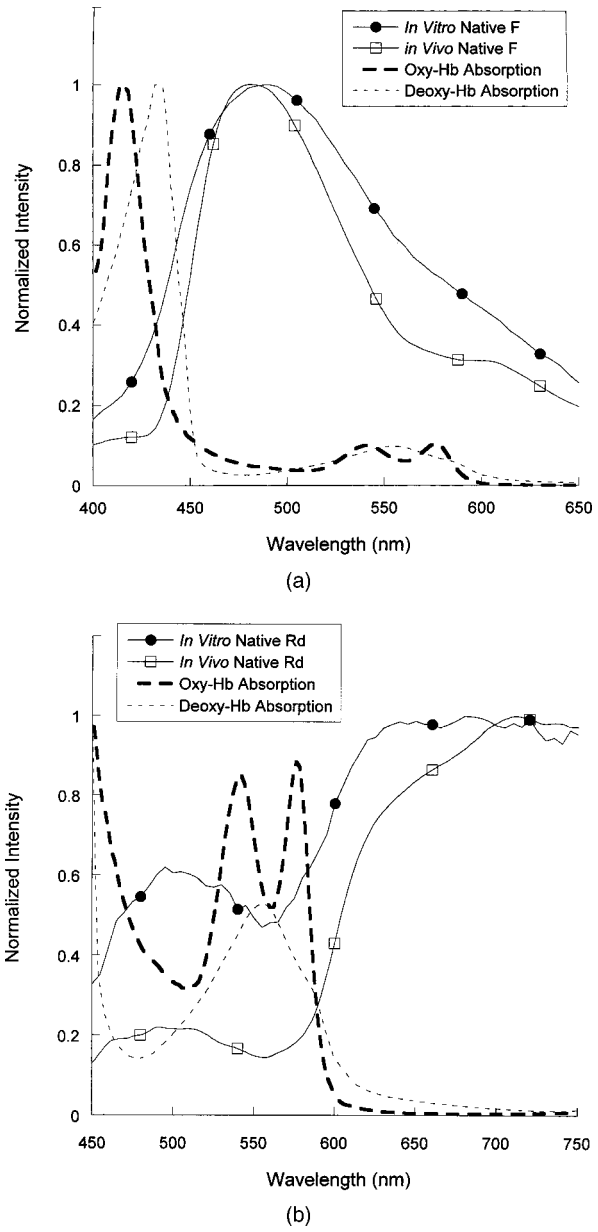

Fig. 7 The comparison of representative *in vitro* and *in vivo* (a) fluorescence and (b) diffuse reflectance spectra from native liver tissue. The optical absorption spectra of oxy- and deoxyhemoglobin are plotted for reference purposes, as many of the features and interspectral differences in the liver spectra can be explained by blood absorption. All spectra are normalized to their peak intensities in this wavelength region.

4 Discussion

In summary, we found that the dominant changes in the fluorescence spectra *in vivo* upon thermal coagulation were a decrease in the peak fluorescence intensity and a shift in the peak toward longer wavelengths. The dominant change in the diffuse reflectance spectra was an increase in intensity across the entire spectral range in question. Spectral features quantifying these changes were found to correlate well with histology, suggesting that optical spectroscopy is a suitable technique for assessing tissue thermal damage.

The reasonably strong correlation between F_{510}/F_{480}, F_{610}/F_{480}, and Rd_{720} and the composite thermal damage score of the samples is significant because it shows that the observed spectral changes are linked to well-understood histological markers of tissue thermal damage, such as hemorrhage, blood coagulation, and tissue whitening.[13] Additionally, the results from the t-test analysis indicate that these spectral correlates of thermal damage are able to differentiate between various histological grades of thermal damage with a reasonable level of confidence. Also, the t-tests reveal that there are performance differences among F_{510}/F_{480}, F_{610}/F_{480}, and Rd_{720}, albeit in this limited sample set. For example, F_{510}/F_{480} and F_{610}/F_{480} appear to be able to differentiate between the intermediate-grade and undamaged/low-grade groups better than Rd_{720}; however, this finding has to be validated in a large-scale study.

The comparison of spectral and histological data, however, is hampered by several problems. First, there is no standardized histological scoring system to grade thermal injury. Second, there is a resolution mismatch between histology and optical spectroscopy in assessing tissue thermal damage. Specifically, the histological technique we used was only capable of separating samples into a few discrete grades of thermal damage, whereas the spectral features we identified could assume a continuous range of values as the tissue progressed from the native condition to a state of severe thermal damage [as shown in Figs. 5(a) and 5(b)]. A histological technique with better accuracy and resolution (i.e., the ability to correctly differentiate more grades of thermal damage) would

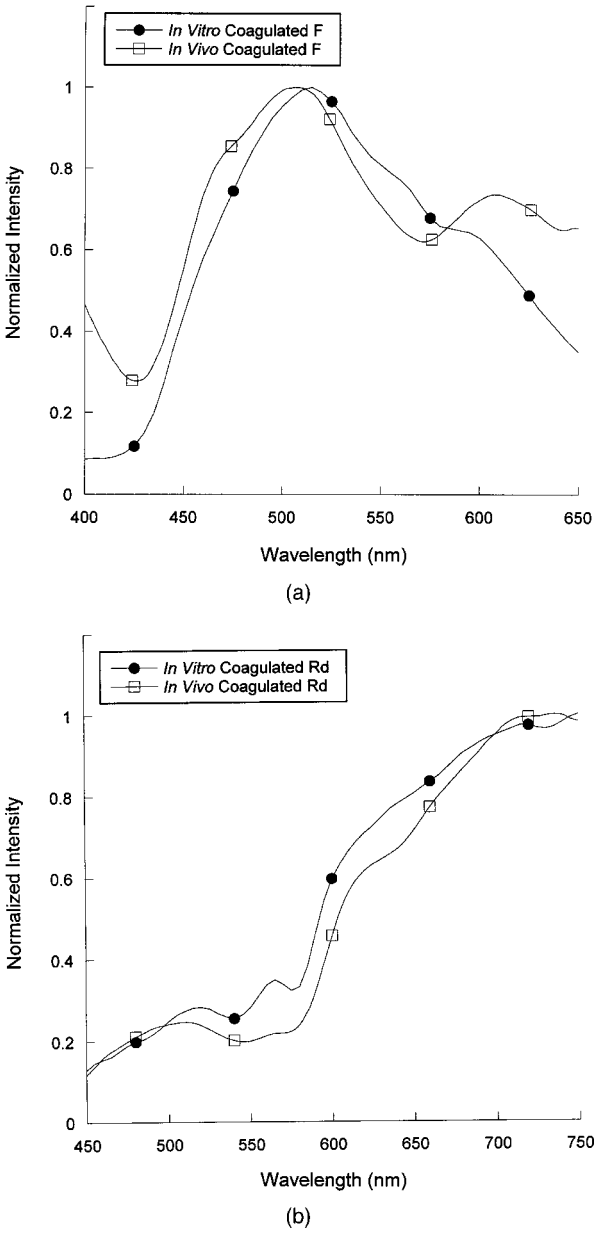

Fig. 8 The comparison of representative *in vitro* and *in vivo* (a) fluorescence and (b) diffuse reflectance spectra from coagulated liver tissue. All spectra are normalized to their peak intensities in this wavelength region.

have likely improved the degree of correlation in the spectral feature versus histology plots (Fig. 6).

Another reason for the scatter in the spectral feature versus histology plots was the inherent inaccuracy of the method used for registering the location of the optical probe tip. The India ink used to register the location of the tip tended to diffuse and ended up staining tissue several millimeters beyond the immediate vicinity of the tip. Furthermore, the thermal damage process and the mechanical deformation introduced by the excision and slicing of the ablation zones tended to damage the optical probe track. A registration error of several millimeters could mean the difference between a location in the hemorrhagic margin of the zone of ablation and the periphery of the necrotic core. As noted previously, incorrect identification of the probe tip location led to large inconsistencies between the histological and spectral data for several fluorescence and diffuse reflectance samples. However, the clear correlation between the histological and spectral data, in spite of the error in localizing the probe tip and the shortcomings of the histological technique and scoring system, testifies to the strength of using optical spectroscopy to assess tissue thermal damage.

One of the key goals of this research is to determine the values of F_{510}/F_{480}, F_{610}/F_{480}, and Rd_{720} (or other spectral correlates) that correspond to tissue death. We suspect that these spectral cut-off values may lie well below the plateau region, which corresponds to the necrotic core of the zone of ablation according to gross histology. The spectral cut-off values would then be used to signify the death of local tissue, and hence determine the endpoint for thermotherapy of liver tumors. However, due to patient-to-patient variability, the absolute value of the spectral correlate may need to be considered, together with other factors such as its time rate of change. The current study shows that in a complete ablation, the spectral correlate does eventually reach a plateau. Therefore, a feedback algorithm could be developed in which the value of the spectral correlate must rise above a certain threshold as well as approach a stable plateau (i.e., a region where its derivative is near zero or below some cut-off value) before therapy is terminated. Animal survival studies are necessary to estimate the spectral correlate value corresponding to tissue death, and to develop and test different algorithms to predict the final volume of coagulative necrosis.

System performance considerations were a factor in selecting appropriate spectral correlates of tissue thermal damage. The pulse-to-pulse energy fluctuation of the nitrogen laser, as well as the pulsed nature of its output, led us to select ratios of fluorescence intensities to represent the observed spectral changes. Using a laser energy meter, it was found that the standard deviation of 1200 laser pulses (20 pps for 1 min) was approximately 15% of the mean pulse energy. Furthermore, because the data acquisition software was not synchronized with the laser trigger, the number of pulses binned during the integration period likely varied by a pulse or two. Stability tests were also performed on the halogen lamp in which its emission spectrum was recorded every 15 s for 5 min. Between 500 and 750 nm, the standard deviation of the intensity was found to be less than 1%. Therefore, it seemed reasonable to use the diffuse reflectance intensity at a single wavelength (e.g., 720 nm) to represent the increase in diffuse reflectance caused by tissue thermal damage. Finally, in our *in vitro* studies,[19] we used Rd_{750} to quantify the changes in the diffuse reflectance spectra. However, in the current system, the combination of poor spectrometer sensitivity and weak halogen lamp emissivity in the near-infrared region led to poor signal-to-noise ratios beyond 750 nm. Rd_{720} was more stable and was therefore used.

The observed increase in the diffuse reflectance intensity is consistent with our *in vitro* results and can be explained by thermally induced changes in tissue optical properties. Data from our lab,[19] as well as numerous other published studies,[23–27] indicate that the dominant change in liver tissue optical properties upon thermal coagulation is an increase in the reduced scattering coefficient (μ_s'). This increase in μ_s'

reflects changes occurring on a cellular and intracellular level, such as protein denaturation, hyalinization of collagen, cytoskeleton collapse, and cell membrane rupture, some of which are known to occur at onset temperatures between 45 and 90 °C.[13] These thermally induced structural changes all affect the size and distribution of scattering particles in the tissue and, consequently, the light distribution. The exact correlation between these morphological changes and alterations in tissue optical characteristics has not yet been determined.

The decrease in the peak fluorescence intensity may be explained by a decrease in penetration depth and local fluence rate at the excitation wavelength (337 nm). Using our *in vitro* optical property measurements,[19] penetration depths for native and coagulated liver tissue were estimated to be ~0.17 and ~0.12 mm, respectively. This, in turn, would lead to a decrease in the volume of tissue being irradiated. Assuming a uniform distribution of fluorophores, the reduction of the interrogation volume translates into a decrease in the total fluorescence emission. Furthermore, thermal damage leads to a decrease in the fluence rate of the excitation light under the collection fibers, according to the predictions of a Monte Carlo simulation model for light propagation. Therefore, the observed decrease in fluorescence intensity may be explained by the synergistic effect of decreased penetration and decreased local fluence rate of the excitation light.

Decrease in fluorescence emission may also be explained by degradation and quantity reduction of fluorophores. It is believed that tissue autofluorescence at 337 nm excitation are originated primary collagen, dihydronicotinamide adenine (phosphate) dinucleotide [NAD(p)H], and flavin adenine dinucleotide (FAD). It is also known that the fluorescence of proteins is due to the interaction of photons of a specific energy with specific chemical bonds (e.g., UV photons with collagen crosslinks).[28] Thermal denaturation of proteins can cause the breaking of those bonds responsible for their fluorescence properties. The interstitial extracellular matrix in liver tissue is known to contain ten different types of collagen, including fibrillar collagens, such as collagen I.[29] It has been shown that the fluorescence emission peak of collagen I at 410 nm (337-nm excitation) decreases dramatically as a function of thermal damage.[30] After 60 min of heating in a 70 °C water bath, a 60% decrease in the fluorescence emission at 410 nm relative to controls was reported.[30] Furthermore, thermal injury alters the biophysiological function of tissue and destroys micro-organelles (e.g., mitochondria) at the microscopic level, which could lead to a reduction in NAD(p)H and FAD quantity in cells and hence fluorescence intensity between 400- and 550-nm emission. In a couple of our recent experimental studies, which have not yet been published, we found that hyperthemia induces reduction of cell fluorescence at 337-nm excitation in a manner similar to that reported in this work, and mitochondrion damage could be clearly seen in tissue samples losing their autofluorescence resulting from thermal damage. Therefore, the observed decrease in overall fluorescence intensity as well as the shift in the fluorescence peak to longer wavelengths in this study may be a combined effect of thermally induced changes in tissue optics and degradation/quantity reduction of fluorophores.

To rule out the possibility that photobleaching or other nonthermal factors were contributing to the changes in F_{510}/F_{480}, F_{610}/F_{480}, and Rd_{720} over the ablation time course, control measurements were made during each dog surgery. F_{610}/F_{480} controls showed no clear trend over the acquisition period and were found to fluctuate very little, with a standard deviation equal to 3 to 4% of the mean. Similar results were obtained for F_{510}/F_{480} and Rd_{720} controls. Again, no clear trends over time were observed and the standard deviations of F_{510}/F_{480} controls were found to be less than 2% of the mean, whereas the standard deviation of Rd_{720} controls were less than 3% of the mean. These results directly support the assertion that the changes in F_{510}/F_{480}, F_{610}/F_{480}, and Rd_{720} are primarily due to tissue thermal damage.

The observed differences in line shape between *in vitro* and *in vivo* native and coagulated spectra can be primarily attributed to increased blood absorption *in vivo*. Hemoglobin is the dominant chromophore in blood, and its absorption spectrum effectively acts as a series of bandpass filters of different degrees, attenuating selected regions of the emission spectrum, and allowing complementary portions of the emission spectrum to propagate through the tissue. In general, it is expected that perfused liver tissue will exhibit stronger blood absorption signatures than nonperfused tissue, since there is a higher concentration of hemoglobin molecules per unit tissue volume in the perfused case. Additionally, the trauma caused by the insertion of the optical probe may cause an additional amount of blood absorption due to pooling of blood around the probe tip. However, since blood oxygenation data were not acquired from the optical interrogation site during surgery, it is impossible to know the relative contributions of oxy- and deoxyhemoglobin absorption. Furthermore, the effect of high-temperature (50 to 100 °C) heating on the oxygenation and light absorption properties of hemoglobin and blood have yet to be studied. Nevertheless, a general explanation of the differences between the *in vitro* and *in vivo* spectra of native samples is possible. For example, the compression along the wavelength axis of the native *in vivo* fluorescence spectrum relative to the corresponding *in vitro* spectrum can be explained by the strong absorption peaks of oxyhemoglobin and deoxyhemoglobin at 414 and 432 nm, respectively and the relatively weaker absorption peaks between 540 and 580 nm [Fig. 7(a)]. Increased blood absorption between 540 and 580 nm also explains the valley in this region in the native *in vivo* diffuse reflectance spectrum [Fig. 8(a)]. Studies are underway in our lab to investigate the effect of heating on the fluorescence and diffuse reflectance spectra of the various components of liver tissue, such as hepatocytes and blood. These studies are necessary to further elucidate the causes of the observed thermally induced spectral alterations.

5 Conclusion

The key findings of this study are that fluorescence and diffuse reflectance spectra can be measured *in vivo* in perfused liver tissue undergoing radio-frequency ablation and that the observed spectral alterations correlate well with histological markers of thermal damage. The observed red shift of the fluorescence peak, decrease in overall fluorescence, and increase in diffuse reflectance upon thermal coagulation are quantified using F_{510}/F_{480}, F_{610}/F_{480}, and Rd_{720}, respectively. The results of this study suggest the potential of using fluorescence and diffuse reflectance spectroscopy as feedback control for thermotherapies of liver tumors.

Acknowledgments

The authors gratefully acknowledge Phil Williams and Amy Nunnally of the Vanderbilt Surgical Research Lab for their assistance with these studies, and RITA Medical Systems for providing the RFA system.

References

1. A. J. Bilchik, T. F. Wood, and D. P. Allegra, ''Radiofrequency ablation of unresectable hepatic malignancies: lessons learned,'' *Oncologist* **6**, 24–33 (2001).
2. S. A. Curley, ''Radiofrequency ablation of malignant liver tumors,'' *Oncologist* **6**, 14–23 (2001).
3. S. A. Curley, F. Izzo, L. M. Ellis, J. Nicolas Vauthey, and P. Vallone, ''Radiofrequency ablation of hepatocellular cancer in 110 patients with cirrhosis,'' *Ann. Surg.* **232**, 381–391 (2000).
4. E. Berber, N. Flesher, and A. E. Siperstein, ''Laparoscopic radiofrequency ablation of neuroendocrine liver metastases,'' *World J. Surg.* **26**, 985–990 (2002).
5. R. Lencioni, O. Goletti, N. Armillotta, A. Paolicchi, M. Moretti, D. Cioni, F. Donati, A. Cicorelli, S. Ricci, M. Carrai, P. F. Conte, E. Cavina, and C. Bartolozzi, ''Radio-frequency thermal ablation of liver metastases with a cooled-tip electrode needle: results of a pilot clinical trial,'' *Eur. Radiol.* **8**, 1205–1211 (1998).
6. S. Rossi, F. Garbagnati, R. Lencioni, H. P. Allgaier, A. Marchiano, F. Fornari, P. Quaretti, G. D. Tolla, C. Ambrosi, V. Mazzaferro, H. E. Blum, and C. Bartolozzi, ''Percutaneous radio-frequency thermal ablation of nonresectable hepatocellular carcinoma after occlusion of tumor blood supply,'' *Radiology* **217**, 119–126 (2000).
7. A. Siperstein, A. Garland, K. Engle, S. Rogers, E. Berber, A. Foroutani, A. String, T. Ryan, and P. Ituarte, ''Local recurrence after laparoscopic radiofrequency thermal ablation of hepatic tumors,'' *Ann. Surg. Oncol.* **7**, 106–113 (2000).
8. P. H. Moller, L. Lindberg, P. H. Henriksson, B. R. Persson, and K. G. Tranberg, ''Temperature control and light penetration in a feedback interstitial laser thermotherapy system,'' *Int. J. Hyperthermia* **12**, 49–63 (1996).
9. K. Orth, D. Russ, J. Duerr, R. Hibst, R. Steiner, and H. G. Beger, ''Thermo-controlled device for inducing deep coagulation in the liver with the Nd:YAG laser,'' *Lasers Surg. Med.* **20**, 149–156 (1997).
10. M. G. Mack, R. Straub, K. Eichler, K. Engelmann, S. Zangos, A. Roggan, D. Woitaschek, M. Bottger, and T. J. Vogl, ''Percutaneous MR imaging-guided laser-induced thermotherapy of hepatic metastases,'' *Abdom. Imaging* **26**, 369–374 (2001).
11. B. Gewiese, J. Beuthan, F. Fobbe, D. Stiller, G. Muller, J. Bose-Landgraf, K. J. Wolf, and M. Deimling, ''Magnetic resonance imaging-controlled laser-induced interstitial thermotherapy,'' *Invest. Radiol.* **29**, 345–351 (1994).
12. F. K. Wacker, K. Reither, J. P. Ritz, A. Roggan, C. T. Germer, and K. J. Wolf, ''MR-guided interstitial laser-induced thermotherapy of hepatic metastasis combined with arterial blood flow reduction: technique and first clinical results in an open MR system,'' *J. Magn. Reson. Imaging* **13**, 31–36 (2001).
13. J. Pearce and S. Thomsen, ''Rate process analysis of thermal damage,'' in *Optical-Thermal Response of Laser-Irradiated Tissue*, A. J. Welch and M. J. C. van Gemert, Eds., pp. 561–606, Plenum Press, New York (1995).
14. J. Leyendecker, G. R. Dodd, G. Halff, V. McCoy, D. Napier, L. Hubbard, K. Chintapalli, S. Chopra, W. Washburn, R. Esterl, F. Cigarroa, R. Kohlmeier, and F. Sharkey, ''Sonographically observed echogenic response during intraoperative radiofrequency ablation of cirrhotic livers: pathologic correlation,'' *AJR, Am. J. Roentgenol.* **178**, 1147–1151 (2002).
15. T. Varghese, J. Zagzebski, Q. Chen, U. Techavipoo, G. Frank, C. Johnson, A. Wright, and F. Lee, ''Ultrasound monitoring of temperature change during radiofrequency ablation: preliminary in-vivo results,'' *Ultrasound Med. Biol.* **28**, 321–329 (2002).
16. S. Raman, D. Lu, D. Vodopich, J. Sayre, and C. Lassman, ''Creation of radiofrequency lesions in a porcine model: correlation with sonography, CT, and histopathology,'' *AJR, Am. J. Roentgenol.* **175**, 1253–1258 (2000).
17. W. M. Whelan, P. Chun, L. C. Chin, M. D. Sherar, and I. A. Vitkin, ''Laser thermal therapy: utility of interstitial fluence monitoring for locating optical sensors,'' *Phys. Med. Biol.* **46**, 91–96 (2001).
18. L. Chin, W. Whelan, M. Sherar, and I. Vitkin, ''Changes in relative light fluence measured during laser heating; implication for optical monitoring and modeling of interstitial laser photocoagulation,'' *Phys. Med. Biol.* **46**, 2407–2420 (2001).
19. W. C. Lin, C. R. Buttemere, and A. Mahadevan-Jansen, ''Effect of thermal damage on the in vitro optical and fluorescence characteristics of hepatic tissues,'' *IEEE J. Sel. Top. Quantum Electron.* **9**(2), 162–170 (2003).
20. W. C. Lin, M. Motamedi, and A. J. Welch, ''Dynamics of tissue optics during laser heating of turbid media,'' *Appl. Opt.* **35**, 3413–3420 (1996).
21. W. H. Press, B. P. Flannery, S. A. Teukolsky, and W. T. Vetterling, *Numerical Recipes in C: The Art of Scientific Computing*, Cambridge University Press, New York (1992).
22. S. Prahl, ''Optical absorption of hemoglobin,'' see http://omlc.ogi.edu/spectra/hrmoglobin/index.html (1999).
23. W. C. Lin, S. A. Toms, M. Motamedi, E. D. Jansen, and A. Mahadevan-Jansen, ''Brain tumor demarcation using optical spectroscopy; an *in vitro* study,'' *J. Biomed. Opt.* **5**, 214–220 (2000).
24. J. P. Ritz, A. Roggan, C. Isbert, G. Muller, H. J. Buhr, and C. T. Germer, ''Optical properties of native and coagulated porcine liver tissue between 400 and 2400 nm,'' *Lasers Surg. Med.* **29**, 205–212 (2001).
25. J. P. Ritz, A. Roggan, C. T. Germer, C. Isbert, G. Muller, and H. J. Buhr, ''Continuous changes in the optical properties of liver tissue during laser-induced interstitial thermotherapy,'' *Lasers Surg. Med.* **28**, 307–312 (2001).
26. J. W. Pickering, P. Posthumus, and M. J. van Gemert, ''Continuous measurement of the heat-induced changes in the optical properties (at 1,064 nm) of rat liver,'' *Lasers Surg. Med.* **15**, 200–205 (1994).
27. C. T. Germer, A. Roggan, J. P. Ritz, C. Isbert, D. Albrecht, G. Muller, and H. J. Buhr, ''Optical properties of native and coagulated human liver tissue and liver metastases in the near infrared range,'' *Lasers Surg. Med.* **23**, 194–203 (1998).
28. R. Richards-Kortum and E. Sevick-Muraca, ''Quantitative optical spectroscopy for tissue diagnosis,'' *Annu. Rev. Phys. Chem.* **47**, 555–606 (1996).
29. D. Schuppan, M. Ruehl, R. Somasundaram, and E. G. Hahn, ''Matrix as a modulator of hepatic fibrogenesis,'' *Semin Liver Dis.* **21**, 351–372 (2001).
30. T. Theodossiou, G. S. Rapti, V. Hovhannisyan, E. Georgiou, K. Politopoulos, and D. Yova, ''Thermally induced irreversible conformational changes in collagen probed by optical second harmonic generation and laser-induced fluorescence,'' *Lasers Med. Sci.* **17**, 34–41 (2002).